

# Impacts of hexadecapole deformations on the collective energy spectra of axially deformed nuclei

L. Lotina<sup>1,\*</sup> and K. Nomura<sup>2,3,†</sup>

<sup>1</sup>*Department of Physics, Faculty of Science, University of Zagreb, HR-10000 Zagreb, Croatia*

<sup>2</sup>*Department of Physics, Hokkaido University, Sapporo 060-0810, Japan*

<sup>3</sup>*Nuclear Reaction Data Center, Hokkaido University, Sapporo 060-0810, Japan*

(Dated: March 7, 2024)

The hexadecapole deformation, as well as the quadrupole one, influences the low-lying states of finite nuclei. The hexadecapole correlations are often overshadowed by the large quadrupole effects, and hence have not been much investigated. Here we address the relevance of hexadecapole deformations in the calculations of low-energy collective states of heavy nuclei, by using the theoretical framework of the self-consistent mean-field method and the interacting-boson approximation. The interacting-boson Hamiltonian that explicitly includes the quadrupole and hexadecapole collective degrees of freedom is specified by a choice of the energy density functional and pairing interaction. In an illustrative application to axially deformed Gd isotopes, it is shown that the inclusion of the hexadecapole degree of freedom does not affect most of the low-spin and low-lying states qualitatively, but that has notable effects in that it significantly improves the description of high-spin states of the ground-state bands of nearly spherical vibrational nuclei and gives rise to  $K^\pi = 4^+$  bands exhibiting strong  $E4$  transitions in strongly deformed nuclei.

## I. INTRODUCTION

Deformation of the nuclear surface and the corresponding collective excitations are a prominent aspect of the atomic nucleus [1]. Among those collective excitation modes that correspond to positive-parity states of nuclei, the dominant and most studied is of quadrupole type, while much less attention has been paid to the next leading order, hexadecapole deformation. This is mostly because the effects of the hexadecapole correlations in nuclear low-lying states are often overshadowed by large quadrupole correlation effects. The hexadecapole correlations, nevertheless, have been shown to be present in many rare-earth [1–5], and actinide [6, 7] nuclei, as well as some light ones [8], and have recently been found in exotic isotopes with an unusual proton to neutron number ratio [9]. Notable hexadecapole effects in nuclear collective structure include the appearance of the low-energy  $K^\pi = 4^+$  bands and enhanced electric hexadecapole ( $E4$ ) transitions. Furthermore, recent hydrodynamic simulation has indicated that the hexadecapole deformation plays a role in modeling heavy ion collisions studied at the Relativistic Heavy Ion Collider [10]. In addition, various nuclear deformation effects, including that of hexadecapole type, should have influences on the predictions of the neutrinoless double decay matrix elements of open shell nuclei [11].

It is, therefore, interesting and timely to study impacts of hexadecapole deformations on nuclear structure in a quantitative and systematic way, using a model that allows for an accurate description of excitation spectra and electromagnetic transition properties of low-lying collective states. Among other nuclear structure models, the

interacting boson model (IBM) [12] has been successful for phenomenological descriptions of low-energy collective excitations in medium-heavy and heavy nuclei. The basic assumption of the IBM is that the nuclear low-lying states are described in terms of  $s$  and  $d$  bosons, which reflect [13] the collective monopole,  $S$  (with spin  $0^+$ ), and quadrupole,  $D$  (spin  $2^+$ ), pairs of valence nucleons, respectively. The IBM should have certain microscopic foundations on the underlying nucleonic dynamics, and attempts have been made to derive the model Hamiltonian from more microscopic nuclear structure calculations [13–16]. In particular, a mapping technique has been developed [15] that links the IBM to the framework of the nuclear energy density functional (EDF). This procedure has been successfully applied to describe quadrupole [15–18] and octupole [19, 20] collective states.

In addition to  $s$  and  $d$  bosons, spin  $4^+$ , or  $g$ , bosons have often been considered in the IBM [12]. The importance of  $g$  bosons in describing spectroscopic properties of deformed nuclei has been addressed from various perspectives [21–31]. Some of these earlier studies also concern the validity of the  $sd$ -IBM from a microscopic point of view, that is, the question as to whether the  $g$  boson degrees of freedom are indispensable or not for a precise description of axially deformed nuclei [21–24, 26]. Along with the strongly deformed regions, it should be also of interest to investigate the significance of the hexadecapole correlation effects in those nuclei in nearly spherical vibrational and transitional regions.

In this article, we implement the hexadecapole ( $g$  boson) degree freedom in the IBM by means of the aforementioned mapping procedure [15], and demonstrate that the hexadecapole effects are present in the low-energy collective states of heavy nuclei in the nearly spherical vibrational region as well as in the strongly deformed region. As an illustrative example we focus on the isotopic chain of axially deformed  $^{148-160}\text{Gd}$  nuclei,

\* [llotina.phy@pmf.hr](mailto:llotina.phy@pmf.hr)

† [nomura@sci.hokudai.ac.jp](mailto:nomura@sci.hokudai.ac.jp)

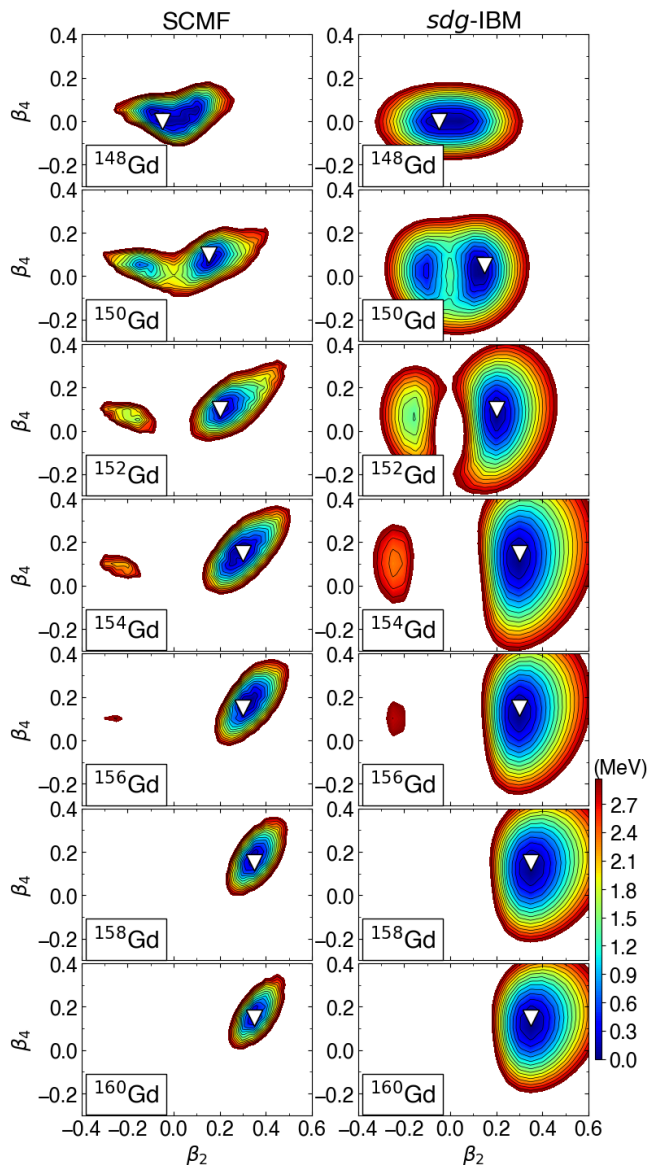


FIG. 1. Left column: axially symmetric quadrupole ( $\beta_2$ ) and hexadecapole ( $\beta_4$ ) constrained energy surfaces for the  $^{148-160}\text{Gd}$  isotopes calculated within the relativistic Hartree-Bogoliubov method using the density-dependent point-coupling energy density functional and the pairing force of finite range. Right column: the corresponding energy surfaces of the  $sdg$ -IBM. The global minimum is indicated by the open triangles.

which exhibits a manifest first-order shape phase transition from spherical to (quadrupole) deformed shapes [32], and for which hexadecapole collectivity has also been suggested to emerge empirically.

## II. SCMF ENERGY SURFACES AND MAPPING ONTO THE IBM

Our analysis begins with the self-consistent mean-field (SCMF) calculations using a nuclear EDF. The nuclear EDF approaches are nowadays among the most reliable theoretical methods of studying intrinsic and excited states of finite nuclei [33–40], and hexadecapole deformations have also been considered as additional collective coordinates (see, e.g., Refs. [10, 41, 42]). For the  $^{148-160}\text{Gd}$  isotopes, we perform the SCMF calculations within the multidimensionally constrained relativistic mean-field (MDC-RMF) model [40, 43] and obtain energy surfaces in terms of the axial quadrupole ( $\beta_2$ ) and hexadecapole ( $\beta_4$ ) deformations, which are shown on the left column of Fig. 1. The SCMF calculations are here carried out within the relativistic Hartree-Bogoliubov framework [36, 38] using the density-dependent point-coupling (DD-PC1) interaction [44] and the separable pairing force of finite range [45]. The constraints are on the expectation values of axial quadrupole  $\hat{Q}_{20}$  and hexadecapole  $\hat{Q}_{40}$  moments, which are related to the deformation parameters  $\beta_2$  and  $\beta_4$  through the relation,  $\beta_\lambda = (4\pi/3AR^\lambda) \langle \hat{Q}_{\lambda 0} \rangle$  with  $\lambda = 2, 4$  and  $R = 1.2A^{1/3}$  fm.

As one can see in Fig. 1, for most of the Gd nuclei, the hexadecapole deformed ground state with a positive  $\beta_4$  value is obtained in the SCMF energy surfaces: the global minimum occurs at the deformations  $(\beta_2^{\min}, \beta_4^{\min}) \approx (-0.05, 0)$ ,  $(0.15, 0.05)$ ,  $(0.2, 0.1)$ ,  $(0.3, 0.15)$ ,  $(0.3, 0.15)$ ,  $(0.35, 0.15)$ , and  $(0.35, 0.15)$  for  $^{148-160}\text{Gd}$ , respectively. Both the  $\beta_2^{\min}$  and  $\beta_4^{\min}$  values keep increasing with the neutron number, but the latter changes more slowly than the former. One notices that there is no  $\beta_4 \neq 0$  minimum on the energy surface of  $^{148}\text{Gd}$ . The potential is nevertheless rather soft along the  $\beta_4$  direction, softest among the considered Gd isotopes. The softness in  $\beta_4$  implies that the hexadecapole correlations play an important role in this nucleus, and, as we show below, to account for the  $\beta_4$  softness the  $g$  boson degree of freedom is required. These findings, regarding the  $\beta_2 - \beta_4$  energy surfaces, are consistent with earlier SCMF results obtained for the same mass region, e.g., the one with the axially deformed Woods-Saxon potential involving the hexadecapole degree of freedom [46], and a more recent beyond-SCMF calculation that is based on the Gogny forces dealing with the quadrupole-hexadecapole coupling [42].

The SCMF results are then used to construct the Hamiltonian of the  $s$ ,  $d$ , and  $g$  boson system (denoted as  $sdg$ -IBM), which gives rise to excitation energies and electromagnetic transition rates. For the  $sdg$ -IBM Hamiltonian, we exploit the form that has been shown to be adequate for phenomenological descriptions of shape phase transitions with quadrupole and hexadecapole degrees of freedom [31]:

$$\hat{H}_{sdg} = \epsilon_d \hat{n}_d + \epsilon_g \hat{n}_g + \kappa \hat{Q} \cdot \hat{Q} + \kappa (1 - \chi^2) \hat{Q}' \cdot \hat{Q}', \quad (1)$$

where the first and second terms in the right-hand side

stand for the  $d$ -, and  $g$ -boson number operators,  $\hat{n}_d = d^\dagger \cdot \tilde{d}$  and  $\hat{n}_g = g^\dagger \cdot \tilde{g}$ , respectively. The third term represents the quadrupole-quadrupole interaction. The quadrupole operator,  $\hat{Q}$ , takes the form

$$\hat{Q} = s^\dagger \tilde{d} + d^\dagger s + \chi \left[ \frac{11\sqrt{10}}{28} (d^\dagger \times \tilde{d})^{(2)} - \frac{9}{7} (d^\dagger \times \tilde{g} + g^\dagger \times \tilde{d})^{(2)} + \frac{3\sqrt{55}}{14} (g^\dagger \times \tilde{g})^{(2)} \right], \quad (2)$$

which is the expression considered also in Ref. [31] and corresponds to a generator of  $sdg$ -SU(3) in the limit  $\chi = 1$  [31, 47]. The last term on the right-hand side of Eq. (1) represents the hexadecapole-hexadecapole interaction, with the hexadecapole operator being  $\hat{Q}' = s^\dagger \tilde{g} + g^\dagger s$ . In principle, the hexadecapole operator in the  $sdg$ -IBM could take a more complicated form that contains some other terms. The reason why we end up with the simplified form that comprises the  $s^\dagger \tilde{g} + g^\dagger s$  terms only is because the SO(15) symmetry is assumed on the  $sdg$ -IBM Hamiltonian (see Refs. [28, 31] for the details). In addition, for the sake of simplicity no distinction is made between the neutron and proton degrees of freedom. While a more realistic study would require that neutron and proton bosons be treated separately, it is expected that there is no qualitative difference in the description of the low-lying yrast states of most of the medium-heavy and heavy nuclei between the IBM that is comprised of neutron and proton bosons and the one in which they are not distinguished. The distinction between neutron and proton bosons would be relevant when describing phenomena such as the neutron-proton mixed symmetry states and the related magnetic dipole properties, in which the neutron and proton degrees of freedom play an important role. On the other hand, the scope of present work is to study the effect of  $g$  bosons on energy spectra, and for the initial application of the mapped  $sdg$ -IBM framework to realistic cases, it would be sufficient to use a simpler version of the  $sdg$ -IBM, where the neutrons and protons are not distinguished.

The parameters of the Hamiltonian (1) ( $\epsilon_d$ ,  $\epsilon_g$ ,  $\kappa$  and  $\chi$ ) are determined, for each nucleus, by applying the method of Ref. [15]: the  $\beta_2 - \beta_4$  SCMF energy surface,  $E_{\text{SCMF}}(\beta_2, \beta_4)$ , is mapped onto the equivalent energy surface of the boson system,  $E_{\text{IBM}}(\tilde{\beta}_2, \tilde{\beta}_4)$ , so that the approximate equality,

$$E_{\text{SCMF}}(\beta_2, \beta_4) \approx E_{\text{IBM}}(\tilde{\beta}_2, \tilde{\beta}_4), \quad (3)$$

should be satisfied in the neighborhood of the global minimum. Here,  $E_{\text{IBM}}(\tilde{\beta}_2, \tilde{\beta}_4)$  is given as the expectation value of the Hamiltonian (1) in the coherent state  $|\phi\rangle$ , with  $|\phi\rangle \propto (1 + \tilde{\beta}_2 d_0^\dagger + \tilde{\beta}_4 g_0^\dagger)^{N_B} |0\rangle$  [28, 48].  $N_B$  stands for the number of bosons, which is equal to half the number of valence nucleons, and the ket  $|0\rangle$  represents the inert core, i.e., the doubly magic nucleus  $^{132}\text{Sn}$ . The amplitudes  $\tilde{\beta}_2$  and  $\tilde{\beta}_4$  stand for the boson analogs of the axial quadrupole and hexadecapole deformations,

respectively, and are assumed to be proportional to the fermionic counterparts, that is,  $\tilde{\beta}_2 \propto \beta_2$  and  $\tilde{\beta}_4 \propto \beta_4$ . See Refs. [15, 16] for further details of this mapping procedure in the case of  $sd$ -IBM.

On the right column of Fig. 1, we show the mapped  $sdg$ -IBM  $\beta_2 - \beta_4$  deformation energy surfaces. One can see that the basic characteristics of the SCMF energy surface, such as the depth of the potential and the coordinates corresponding to the global minimum  $[(\beta_2^{\text{min}}, \beta_4^{\text{min}})]$ , are reproduced in the mapped  $sdg$ -IBM surfaces.

To compare with the  $sdg$ -IBM results, we also carry out the calculations within the original version of the IBM, that comprises  $s$  and  $d$  bosons only ( $sd$ -IBM). The  $sd$ -IBM Hamiltonian here takes the standard form [12]

$$\hat{H}_{sd} = \epsilon_d \hat{n}_d + \kappa \hat{Q}_{sd} \cdot \hat{Q}_{sd}, \quad (4)$$

where  $\hat{Q}_{sd} = s^\dagger \tilde{d} + d^\dagger s + \chi_d (d^\dagger \times \tilde{d})^{(2)}$  is the quadrupole operator for the  $(s, d)$ -boson systems. The three parameters,  $\epsilon_d$ ,  $\kappa$ , and  $\chi_d$ , are determined by mapping the SCMF energy surface along the  $\beta_2$  deformation with  $\beta_4 = 0$  onto that of the  $sd$ -IBM, that is,  $E_{\text{SCMF}}(\beta_2, \beta_4 = 0) \approx E_{\text{IBM}}^{sd}(\beta_2)$ .

### III. RESULTS

Figure 2(a) and 2(b) show the excitation energies of even-spin positive-parity states in the ground-state bands of  $^{148-160}\text{Gd}$ , obtained from the diagonalization [50] of the mapped  $sd$ - and  $sdg$ -IBM Hamiltonians, respectively, compared to the corresponding experimental data [49]. A noticeable influence of including the hexadecapole deformation on the ground-state bands is that the excitation energies of the states with spin  $I^\pi \geq 6^+$  calculated within the  $sdg$ -IBM for those nuclei with  $N = 84$  and  $86$ , which are close to the neutron magic number  $N = 82$ , are much lower than in the  $sd$ -IBM, and are in agreement with experiment.

The calculated ratios of the first  $4^+$  to  $2^+$  excitation energies,  $R_{4/2} = E_x(4_1^+)/E_x(2_1^+)$ , obtained from the  $sd$  ( $sd$ ) IBM are, 1.86 (2.13), 2.15 (2.18), 2.38 (2.36), 2.84 (2.83), 2.99 (3.08), 3.10 (3.24), 3.16 (3.23) for  $^{148-160}\text{Gd}$ , respectively. The observed  $R_{4/2}$  ratios, on the other hand, are equal to 1.81, 2.02, 2.19, 3.02, 3.24, 3.26, and 3.32 for  $^{148-160}\text{Gd}$ , respectively [49]. By comparing the theoretical and experimental  $R_{4/2}$  ratios, it turns out that another significant impact of  $g$  bosons is that the  $sdg$ -IBM reproduces the experimental  $R_{4/2}$  ratio for the  $^{148}\text{Gd}$  nucleus,  $R_{4/2} = 1.81 < 2$ . The experimental value of  $R_{4/2} < 2$  could be reproduced only by the inclusion of  $g$  bosons, since it lowers the  $4_1^+$  level to be close in energy to the  $2_1^+$  one. The fact that the observed  $R_{4/2}$  ratio for  $^{148}\text{Gd}$  is lower than two also reflects, to a good extent, the contribution from the single-particle excitations, which appear to be effectively accounted for by the inclusion of  $g$  bosons.

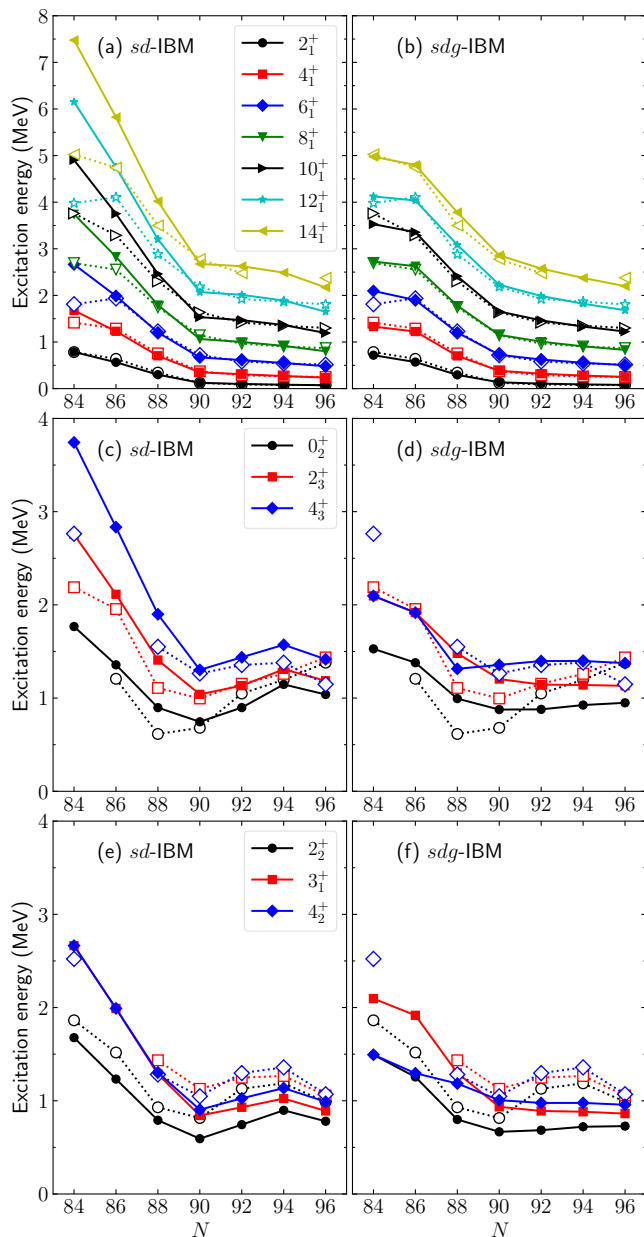


FIG. 2. Energy spectra of positive-parity even-spin yrast states [panels (a) and (b)],  $0_2^+$ ,  $2_3^+$ , and  $4_3^+$  states [panels (c) and (d)], and  $2_2^+$ ,  $3_1^+$ , and  $4_2^+$  states [panels (e) and (f)] of  $^{148-160}\text{Gd}$  calculated with the *sd*- (left column), and *sdg*-IBM (right column) in comparison with the experimental data [49]. The calculated excitation energies are represented by filled symbols, and the corresponding experimental data by the open symbols.

Even though  $g$  bosons, as well as  $s$  and  $d$  bosons, are considered as collective in nature, the fact that the inclusion of  $g$  bosons in the IBM significantly improves description of the observed energy ratio of  $R_{4/2} < 2$ , as well as the fact that the ground-state yrast levels with  $I \geq 6$  is reproduced quite well, indicates that  $g$  bosons

are considered as necessary building blocks to describe the low-energy excitations in the nuclei with  $N = 84$  and  $86$ , where single-particle degrees of freedom come to play a role. We also note that both the *sd*-IBM and *sdg*-IBM have often been applied to nearly spherical and moderately deformed nuclei with  $N$  being near shell closure, and has been shown to be valid in a number of phenomenological applications and in the microscopic considerations.

The lowering of the higher spin levels of the ground-state bands for the nearly spherical nuclei is explained by the increasing  $g$  boson contribution to the wave functions as a function of spin. The contribution of  $g$  bosons to a given state is inferred from the expectation value,  $\langle \hat{n}_g \rangle$ , computed by using the *sdg*-IBM wave function of that state. For  $^{148}\text{Gd}$ , in particular, the states with spin  $I^\pi = 4_1^+$ ,  $6_1^+$ ,  $8_1^+$ , and  $10_1^+$  are shown to contain one  $g$  boson, i.e.,  $\langle \hat{n}_g \rangle \approx 1$ , and  $\langle \hat{n}_g \rangle \approx 1.5$  for the  $12_1^+$ , and  $14_1^+$  states.

Figures 2(c) and 2(d) depict the  $0_2^+$ ,  $2_3^+$ , and  $4_3^+$  energy levels, which are supposed to be part of the excited  $K^\pi = 0^+$  band in the well deformed isotopes with  $N \geq 90$ . The inclusion of  $g$  bosons has an effect of lowering the  $2_3^+$  and  $4_3^+$  energy levels for those nuclei with  $N \leq 88$ . In particular, for the  $4_3^+$  states of  $^{148}\text{Gd}$ ,  $^{150}\text{Gd}$ , and  $^{152}\text{Gd}$  the expectation values are calculated as  $\langle \hat{n}_g \rangle \approx 1$ . On the other hand, the hexadecapole deformation makes only a minor effect on the  $0_2^+$  energy levels in general, as the expectation values  $\langle \hat{n}_g \rangle \approx 0$ . Overall it appears that the *sdg*-IBM does not improve the description of these non-yrast states, and that even the *sd*-IBM, i.e., the calculation without  $g$  bosons, is able to reproduce the observed behaviors of these states rather well.

Figures 2(e) and 2(f) show the excitation spectra of the  $2_2^+$ ,  $3_1^+$ , and  $4_2^+$  states, which are attributed to members of the  $\gamma$  vibrational band. The  $g$  boson effect appears to be minor in the description of the bandhead  $2_2^+$  level, but significantly lowers the energies of the  $3_1^+$  and  $4_2^+$  states for those nuclei with  $N \leq 88$ , which are weakly quadrupole and hexadecapole deformed. Particularly at  $N = 84$ , the  $4_2^+$  level obtained from the *sdg*-IBM is so low in energy as to be close to the  $2_2^+$  level, in comparison to experiment.

The discrepancies between the calculated and experimental energy spectra for nonyrast states, as observed in Figs. 2(c), 2(d), 2(e), and 2(f), are not surprising, given that, unlike the conventional IBM calculations, the Hamiltonian parameters are here not obtained from experiment, but from the mapping of the  $\beta_2 - \beta_4$  SCMF energy surface computed with the EDF that is not tailored for particular nuclei.

The detailed band structure of each nucleus can also be studied. As a representative case we show in Fig. 3 the low-energy positive-parity bands of  $^{154}\text{Gd}$ . In the *sdg*-IBM spectra, states are classified into bands according to the dominant inband  $E2$  transitions and according to the nature of the states in terms of the  $g$ -boson content in their wave functions. One sees from Fig. 3 that the ground-state band is reproduced well. The predicted

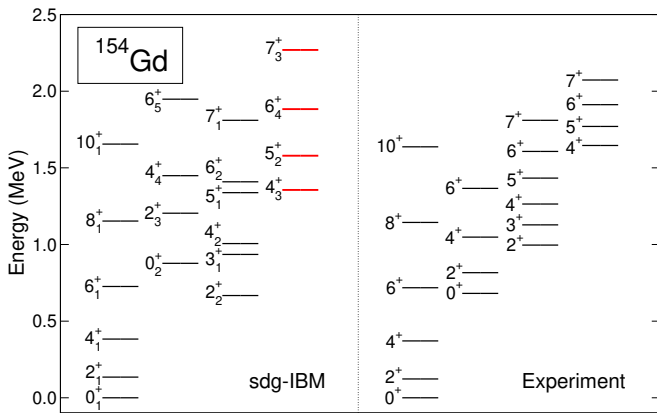


FIG. 3. Low-spin part of the positive-parity bands of  $^{154}\text{Gd}$  calculated with the *sdg*-IBM, in comparison with the experimental data [49]. The theoretical band that is built on the  $4_3^+$  state, highlighted in thick lines with color red, is predicted to be of one-*g*-boson character.

$K^\pi = 0_2^+$  band looks stretched in energy as compared to the experimental one, even though the  $0_2^+$  bandhead energy is reasonably reproduced. The predicted  $\gamma$  band, starting from the  $2_2^+$  state, is much lower in energy than the experimental one. The appearance of the low-lying  $2_2^+$  state indicates too pronounced  $\gamma$  softness, which could be attributed to the particular choice of the nuclear EDF and pairing interaction. In addition, the calculated  $\gamma$  band exhibits a staggering of levels,  $(3_\gamma^+, 4_\gamma^+)$ ,  $(5_\gamma^+, 6_\gamma^+)$ , ... It is a characteristic of a  $\gamma$ -unstable rotor [51], but contradicts the observed feature of the  $\gamma$  band, which looks rather harmonic. To remedy this, cubic terms are often included in the boson Hamiltonian [18], since they lower the energy levels of the odd-spin members of the  $\gamma$  band, to be consistent with the observed  $\gamma$ -band structure that is harmonic. The cubic terms, however, would also lower the  $2^+$  bandhead energy of the  $\gamma$  band, which would become much lower than the experimental counterpart. Such an extension is well beyond the scope of this paper.

The theoretical band, built on top of the  $4_3^+$  state, is interpreted as the  $K^\pi = 4^+$  band and is found to be of one-*g*-boson character in the present calculation. The experimental counterpart is the one with the bandhead energy  $E_x(4_4^+) = 1646$  keV [49].  $E4$  transition properties are calculated with the transition operators that are given by  $e_{4,sg} [\hat{Q}^\dagger + (d^\dagger \times \tilde{d})^{(4)}]$  for the *sdg*-IBM, and  $e_{4,sd} (d^\dagger \times \tilde{d})^{(4)}$  for the *sd*-IBM. The addition of the  $(d^\dagger \times \tilde{d})^{(4)}$  term to the  $E4$  transition operator for the *sdg*-IBM is to compare the impact of *d* bosons to that of *g* bosons on the  $E4$  transitions, and in that way one would be able to see properly how much the presence of *g* bosons affects the  $E4$  transitions. The effective boson charges,  $e_{4,sg}$  and  $e_{4,sd}$ , are fixed to reproduce an available experimental [49]  $B(E4; 4_1^+ \rightarrow 0_1^+)$  transi-

tion rate of  $38 \pm 3$  Weisskopf units (W.u.). The *sd*-IBM gives band structure of  $^{154}\text{Gd}$  qualitatively similar to that with the *sdg*-IBM. The  $K^\pi = 4^+$  band is also obtained in the *sd*-IBM with the bandhead  $4_4^+$  state at the excitation energy of 1412 keV. A significant difference between the *sd*- and *sdg*-IBM predictions is that the  $B(E4; 4_{K=4^+}^+ \rightarrow 0_1^+)$  transition obtained from the former is much lower (1.3 W.u.) than that from the latter (93 W.u.). Experiments to deduce the reduced  $E4$  matrix elements,  $|\langle 0_1^+ || M(E4) || 4_1^+ \rangle|$ , were performed, e.g., in [4, 5], using the  $(\alpha, \alpha')$  scattering and Coulomb excitations, and these transition matrix elements can be used to fix the boson effective charges,  $e_{4,sd}$  and  $e_{4,sg}$ . However, experimental information about other  $E4$  transitions is not available for the Gd isotopes under study, and hence the detailed comparison of the present model with the experimental  $E4$  transition rates is not feasible. An extensive study of the  $E4$  properties in other isotopic chains will be reported elsewhere.

In the deformed region, the improvement of the *sdg*-IBM over the *sd*-IBM is also visible in the higher-lying states of a given spin. For even-spin states, for example, the sixth  $2^+$  state and higher become lower and closer to each other in energy which is in a better agreement with experiment. For odd-spin states, this is even visible, e.g., for the third  $3^+$  state and higher. However, the corresponding experimental data for the  $3^+$  states are scarce. The *sdg*-IBM gives a slightly better description of the in-band  $E2$  transitions,  $I \rightarrow I - 2$ , within ground-state band for high-spin states, e.g.,  $I = 8^+$  and  $10^+$ , for deformed Gd nuclei. There is, on the other hand, no qualitative difference in the calculated  $E0$ , as well as  $E2$ , transition properties for the low-spin states between the *sd*-IBM and *sdg*-IBM. These properties will be discussed in detail in a forthcoming longer article.

#### IV. SUMMARY

To summarize, we have analyzed the impacts of hexadecapole deformations on the low-lying collective states of axially symmetric heavy nuclei in the spherical vibrational as well as strongly deformed regimes. By using the results of the mean-field calculations based on the relativistic EDF, the *sdg*-IBM Hamiltonian has been determined without any adjustment to experiment. The inclusion of *g* bosons has been shown to lower the states of ground-state bands with spin  $I^\pi \geq 6^+$ , especially in the region near the neutron closed shell  $N = 82$ , thus improving the description of vibrational nuclei. For those nuclei with large quadrupole deformation, i.e., with  $N \geq 90$ , the *sdg*-IBM produces the  $K^\pi = 4^+$  band of one-*g*-boson character, which exhibits a much larger  $B(E4; 4_{K^\pi=4^+}^+ \rightarrow 0_1^+)$  transition than in the *sd*-IBM. On the other hand, the *g*-boson effects on low-spin non-yrast states have been shown to be marginal for most of the deformed nuclei, in which cases the *sd*-IBM appears to reproduce the experimental data rather well. Now that we

have a way of incorporating the quadrupole and hexadecapole degrees of freedom in the IBM in a unified manner, it can be applied to identify regions of the nuclear chart, including the experimentally unexplored ones, in which hexadecapole correlations may play prominent roles.

## ACKNOWLEDGMENTS

The work of L.L. is financed within the Tenure Track Pilot Programme of the Croatian Science Foundation and

the École Polytechnique Fédérale de Lausanne, and the project TTP-2018-07-3554 Exotic Nuclear Structure and Dynamics, with funds from the Croatian-Swiss Research Programme.

- 
- [1] A. Bohr and B. R. Mottelson, *Nuclear Structure*, Vol. II (Benjamin, New York, USA, 1975).
- [2] D. Hendrie, N. Glendenning, B. Harvey, O. Jarvis, H. Duhm, J. Saudinos, and J. Mahoney, *Phys. Lett. B* **26**, 127 (1968).
- [3] K. A. Erb, J. E. Holden, I. Y. Lee, J. X. Saladin, and T. K. Saylor, *Phys. Rev. Lett.* **29**, 1010 (1972).
- [4] H. Wollersheim and T. W. Elze, *Nucl. Phys. A* **278**, 87 (1977).
- [5] R. M. Ronningen, J. H. Hamilton, L. Varnell, J. Lange, A. V. Ramayya, G. Garcia-Bermudez, W. Lourens, L. L. Riedinger, F. K. McGowan, P. H. Stelson, R. L. Robinson, and J. L. C. Ford, *Phys. Rev. C* **16**, 2208 (1977).
- [6] C. E. Bemis, F. K. McGowan, J. L. C. Ford, W. T. Milner, P. H. Stelson, and R. L. Robinson, *Phys. Rev. C* **8**, 1466 (1973).
- [7] N. Zamfir, G. Hering, R. Casten, and P. Paul, *Phys. Lett. B* **357**, 515 (1995).
- [8] Y. Gupta, B. Nayak, U. Garg, K. Hagino, K. Howard, N. Sensharma, M. Şenyiğit, W. Tan, P. O'Malley, M. Smith, R. Gandhi, T. Anderson, R. deBoer, B. Frentz, A. Gyurjinyan, O. Hall, M. Hall, J. Hu, E. Lamere, Q. Liu, A. Long, W. Lu, S. Lyons, K. Ost典ek, C. Seymour, M. Skulski, and B. Vande Kolk, *Phys. Lett. B* **806**, 135473 (2020).
- [9] M. Spieker, S. Agbemava, D. Bazin, S. Biswas, P. Cottle, P. Farris, A. Gade, T. Ginter, S. Giraud, K. Kemper, J. Li, W. Nazarewicz, S. Noji, J. Pereira, L. Riley, M. Smith, D. Weisshaar, and R. Zegers, *Physics Letters B* **841**, 137932 (2023).
- [10] W. Ryssens, G. Giacalone, B. Schenke, and C. Shen, *Phys. Rev. Lett.* **130**, 212302 (2023).
- [11] J. Engel and J. Menéndez, *Rep. Prog. Phys.* **80**, 046301 (2017).
- [12] F. Iachello and A. Arima, *The interacting boson model* (Cambridge University Press, Cambridge, 1987).
- [13] T. Otsuka, A. Arima, and F. Iachello, *Nucl. Phys. A* **309**, 1 (1978).
- [14] T. Mizusaki and T. Otsuka, *Prog. Theor. Phys. Suppl.* **125**, 97 (1996).
- [15] K. Nomura, N. Shimizu, and T. Otsuka, *Phys. Rev. Lett.* **101**, 142501 (2008).
- [16] K. Nomura, N. Shimizu, and T. Otsuka, *Phys. Rev. C* **81**, 044307 (2010).
- [17] K. Nomura, T. Otsuka, N. Shimizu, and L. Guo, *Phys. Rev. C* **83**, 041302 (2011).
- [18] K. Nomura, N. Shimizu, D. Vretenar, T. Nikšić, and T. Otsuka, *Phys. Rev. Lett.* **108**, 132501 (2012).
- [19] K. Nomura, D. Vretenar, and B.-N. Lu, *Phys. Rev. C* **88**, 021303 (2013).
- [20] K. Nomura, D. Vretenar, T. Nikšić, and B.-N. Lu, *Phys. Rev. C* **89**, 024312 (2014).
- [21] A. Bohr and B. R. Mottelson, *Phys. Scr.* **22**, 468 (1980).
- [22] T. Otsuka, *Nucl. Phys. A* **368**, 244 (1981).
- [23] T. Otsuka, A. Arima, and N. Yoshinaga, *Phys. Rev. Lett.* **48**, 387 (1982).
- [24] D. R. Bes, R. A. Broglia, E. Maglione, and A. Vitturi, *Phys. Rev. Lett.* **48**, 1001 (1982).
- [25] P. Van Isacker, K. Heyde, M. Waroquier, and G. Wenes, *Nucl. Phys. A* **380**, 383 (1982).
- [26] T. Otsuka and J. N. Ginocchio, *Phys. Rev. Lett.* **55**, 276 (1985).
- [27] T. Otsuka and M. Sugita, *Phys. Lett. B* **215**, 205 (1988).
- [28] Y. D. Devi and V. K. B. Kota, *Z. Phys. A* **337**, 15 (1990).
- [29] S. Kuyucak, *Nucl. Phys. A* **570**, 187 (1994).
- [30] S. Zerguine, P. Van Isacker, A. Bouldjedri, and S. Heinze, *Phys. Rev. Lett.* **101**, 022502 (2008).
- [31] P. Van Isacker, A. Bouldjedri, and S. Zerguine, *Nucl. Phys. A* **836**, 225 (2010).
- [32] P. Cejnar, J. Jolie, and R. F. Casten, *Rev. Mod. Phys.* **82**, 2155 (2010).
- [33] P. Ring and P. Schuck, *The Nuclear Many-Body Problem* (Springer-Verlag, Berlin, 1980).
- [34] M. Bender, P.-H. Heenen, and P.-G. Reinhard, *Rev. Mod. Phys.* **75**, 121 (2003).
- [35] L. M. Robledo, T. R. Rodríguez, and R. R. Rodríguez-Guzmán, *J. Phys. G: Nucl. Part. Phys.* **46**, 013001 (2019).
- [36] D. Vretenar, A. V. Afanasjev, G. A. Lalazissis, and P. Ring, *Phys. Rep.* **409**, 101 (2005).
- [37] J. Meng, H. Toki, S. Zhou, S. Zhang, W. Long, and L. Geng, *Prog. Part. Nucl. Phys.* **57**, 470 (2006).
- [38] T. Nikšić, D. Vretenar, and P. Ring, *Prog. Part. Nucl. Phys.* **66**, 519 (2011).
- [39] J. Meng and S. G. Zhou, *J. Phys. G: Nucl. Part. Phys.* **42**, 093101 (2015).
- [40] S.-G. Zhou, *Phys. Scr.* **91**, 063008 (2016).
- [41] G. Lalazissis, S. Raman, and P. Ring, *At. Data Nucl. Data Tables* **71**, 1 (1999).
- [42] C. V. N. Kumar and L. M. Robledo, *Phys. Rev. C* **108**, 034312 (2023).
- [43] B.-N. Lu, J. Zhao, E.-G. Zhao, and S.-G. Zhou, *Phys. Rev. C* **89**, 014323 (2014).

- [44] T. Nikšić, D. Vretenar, and P. Ring, *Phys. Rev. C* **78**, 034318 (2008).
- [45] Y. Tian, Z. Y. Ma, and P. Ring, *Phys. Lett. B* **676**, 44 (2009).
- [46] W. Nazarewicz and P. Rozmej, *Nucl. Phys. A* **369**, 396 (1981).
- [47] V. K. B. Kota, J. Van der Jeugt, H. De Meyer, and G. Vanden Berghe, *J. Math. Phys.* **28**, 1644 (1987).
- [48] J. N. Ginocchio and M. W. Kirson, *Nucl. Phys. A* **350**, 31 (1980).
- [49] Brookhaven National Nuclear Data Center, <http://www.nndc.bnl.gov>.
- [50] S. Heinze, computer program ARBMODEL, University of Cologne (2008).
- [51] L. Wilets and M. Jean, *Phys. Rev.* **102**, 788 (1956).